On the Analysis of Switched-Beam Antennas for the W-CDMA Downlink

Ben Allen, *Member, IEEE,* and Mark Beach, *Associate Member, IEEE*

***Abstract*—Smart antennas are widely recognized as an enabling technology for addressing the demand of future wireless network capacity when employed in place of traditional fixed-coverage sector antennas. Furthermore, switched-beam antenna systems offer a robust implementation against multipath propagation effects and reduced complexity that is inherent with fully adaptive implementations. This paper introduces a simple closed-form expression for evaluating the capacity increase of W-CDMA cellular networks employing switched-beam antennas. The expression incorporates the effect of practical antenna patterns and the impact of multipath scattering on code orthogonality, as well as that of pilot signal power. The results show that a reduction in downlink interference of approximately 6 dB can be achieved by installing an eight-beam antenna system in a 120° sector configuration when representative values of these parameters are taken into account.**

***Index Terms*—Antenna arrays, beamforming, code-division multiple-access (CDMA), digital cellular systems, smart antennas, switched-beam antennas, third-generation wireless systems.**

I. Introduction

DEMAND for the provision of multi-media services "anytime, anywhere" continues to grow. Consequently, the quantity of user traffic delivered over wireless networks is set to increase. Advanced modulation, coding, and protocols are solutions that address the wireless capacity demand; however, in addition to these well-recognized techniques, advanced antenna systems, or *smart antennas*, also offer a significant increase in wireless network capacity [1].

A smart antenna operating as a beamformer enables the interference level of cochannel users to be controlled through the spatial filtering process. Such antenna systems can be fully adaptive where the complex weights are automatically adjusted until an optimum solution is reached [2].

One simple alternative to the fully adaptive antenna is the switched-beam architecture in which the best beam is chosen from a number of fixed steered beams. Such antennas are considered by many to be a robust and cost-effective method of increasing capacity in cellular networks [3], [4]. Switched-beam systems [5]–[8] are technologically the simplest and can be implemented by using a number of fixed, independent, or directional antennas or with an antenna array and analog beamformer

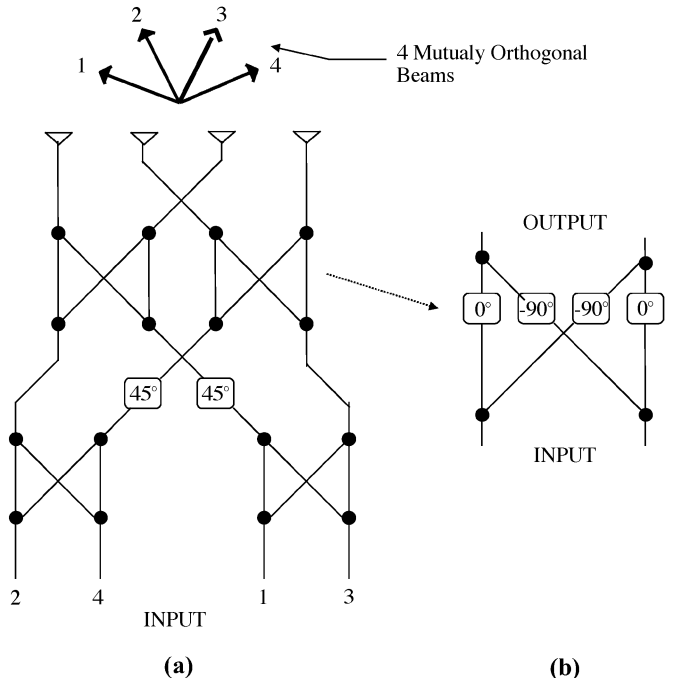

Fig. 1. Butler matrix. (a) 4 × 4 Butler matrix. (b) A hybrid used to form a Butler matrix.

such as a Butler matrix [9]–[11] or Rotman lens [12]. Fig. 1(a) shows the basic architecture of a four-port Butler matrix that consists of four hybrid couplers, which are shown in Fig. 1(b). The system is easily expanded to support eight beams by repeating the apparent pattern for a further four ports. The operation of a Butler matrix can be likened to a fast Fourier transform and yields M mutually orthogonal beams.

A similar technique called *grid of beams* (GOB) can be used with digital beamforming systems, which selects the appropriate weight vector from a stored set. This, however, leads to a more complex implementation due to the drawbacks associated with digital beamforming that are highlighted in [13] and [14]. GOB does not require the beams to be orthogonal, enabling the beam cusp to be adjusted and an arbitrary number of beams can be formed, each of 3-dB beamwidth $(\theta_{3\text{ dB}})$, given by

$$\theta_{3\text{ dB}} = \frac{0.886 \cdot \lambda}{M \cdot d \cdot \cos(\theta_o)} \tag{1}$$

(assuming uniform array amplitude weighting) [15].

Where M = number of elements, d = element spacing, λ = free space wavelength, and θ_o is the steering angle from

Manuscript received March 27, 2002; revised January 6, 2003, November 18, 2003, and December 9, 2003.

B. Allen is with the Centre for Telecommunications Research, King's College, Strand, London, WC2R 2LS, U.K. (e-mail: Ben.Allen@kcl.ac.uk).

M. Beach is with Centre for Communications Research, University of Bristol, Bristol, BS8 1UB, U.K. (e-mail: M.A.Beach@bristol.ac.uk).

Digital Object Identifier 10.1109/TVT.2004.825782

boresight. Furthermore, applying a window function such as a Hanning or Hamming window can control the sidelobe levels. A GOB beamformer was implemented in the TSUNAMI II field trials system, which used 11 beams distributed over a 120° sector [13]. The results obtained in the reference show that this technique was unsuitable in interference-limited systems as the unwanted and wanted signal sources could not be identified when beams are selected on a best receiver signal-strength indicator (RSSI) basis. However, an extension to this technique reported in [13], [16], and [17] overcomes this by using training sequences or user color codes to distinguish between users. In [17], a carrier-to-interference ratio (CIR) improvement of between 1 and 4 dB using a four-beam system is reported, with the best improvement occurring at high received signal-to-noise-plus-interference ratios.

Switched-beam systems implemented using a Butler matrix or radio-frequency (RF) beamforming network also have the advantage of being able to be a direct replacement for existing diversity systems. This enables wireless operators to perform equipment upgrades in order to address the steady growth in subscriber numbers, rather than coordinating a completely new equipment rollout. They can also offer computational stability in multipath environments and enhance services to network *hot spots* [18], [19].

An interesting phenomenon reported in [20] is the *cartwheel effect*, which describes the nonuniform uplink C/I distribution throughout the cell. This is caused by radial sectors of low C/I that point directly at the first tier of cochannel base stations. Two solutions are proposed to mitigate this effect: dynamic channel assignment and realigning the beams to redistribute the bad areas. The reference also reports on simulation results of a switched-beam system in a time-division multiple-access (TDMA) network. The uplink results show a 2-dB coverage improvement with respect to a 120° sector two-branch space-diversity system.

Reference [19] reports on a switch-beam trials system deployed in a dense urban environment. The four-beam 40° beamwidth system yielded a 3-dB C/I improvement over an omnisector antenna. Here, a nonorthogonal beam set was used to reduce the cusping loss by 3 dB and beams were selected on a best-received signal-strength basis.

Transmit, or downlink beamforming, provides additional challenges to the system designer when operating a frequency-division duplex (FDD) system [21], [22]. By way of an alternative to the fully adaptive computationally intensive downlink beamforming approaches that are necessary when operating over large FDD frequency offsets, a switched-beam system is considered in this contribution. The system architecture is identical to that of an uplink switched-beam system such as that shown in Fig. 1. Tirrola and Ylitalo have appraised a system using two beams over a 120° sector based on a two-port Butler matrix [23]. In the reference, the downlink beam is selected corresponding to the uplink beam that gives the highest received signal strength. Results show a performance improvement for channels where the angular spread is considerably less than the beamwidth. The authors also conclude that two beams per sector is not sufficient, as cusping loss impairs service to users located in this region.

The key advantages of these systems over fully adaptive solutions are as follows.

- *Inherent numerical stability*. This system does not require intense signal processing since beam selection can be based on RF, analog signal processing, and simple control logic. Consequently, algorithm robustness usually is not a design issue.
- *Considerable reduction in computational overhead and delay*. As stated above, complex signal-processing algorithms are not required.
- *Simple implementation*. These systems can be retrofitted to existing cell sites without the complexity associated with digital or adaptive beamforming schemes, which require calibration.

Furthermore, a minimum isolation between cochannel users of approximately 13 dB is achievable (indicated by the side-lobe levels of the beam pattern), whereas fully adaptive techniques can suffer from poor null depth or high side lobes due to angular spread and nonideal array calibration. Hence, there is no "degree-of-freedom" limitation in switched-beam systems when they are subject to high user densities.

The simulation results reported in [20] have shown an area-outage improvement of more than 10 dB above an omnisector antenna when a four-beam 30° beamwidth switched-beam system is deployed in a macrocellular environment. Mootri, Stützle, and Paulraj reported a capacity gain of four to five times that of a standard sectorized IS-95 forward link in [24] when a 12-beam system is employed. The field trials reported in [19] showed a 3-dB improvement in the downlink carrier-to-interference ratio for a similar system. Furthermore, a GOB system was implemented in the TSUNAMI II field-trials system [13]. A mean received power gain of 14.7 dB above a single element system was recorded for this configuration.

In this paper, an extended form of the analysis presented in [25] is given, verifying the performance of a switched-beam antenna system as a downlink (transmit) beamformer in a FDD cellular network. A closed-form expression is introduced, which enables the downlink performance of a number of switched-beam architectures to be evaluated. Unlike previous work that has been reported in the literature, the expression enables the impact of shadowing, code orthogonality, practical beam patterns, and pilot signal transmissions to be assessed. Additionally, this analytical framework allows performance to be assessed without the need for extensive Monte Carlo style simulations. The additional characteristics incorporated in the analysis enables features specific to wideband code-division multiple-access (W-CDMA) systems [26] and hardware specifications to be appraised.

This paper is organized as follows. Section II defines the primary parameters that impact switched-beam antenna performance and that are appraised in the subsequent analysis. Section III develops a closed-form expression that enables system performance to be compared with omnisector base station antennas. The expression incorporates the terms defined in Section II. Section IV presents the performance of switched-beam antenna systems using the analytical expressions. Finally, Section V discusses the results in the context of the given operating conditions.

II. Definition of Terms

The following terms are incorporated in the subsequent analysis of the switched-beam architecture on the downlink of a W-CDMA network.

Loss-of-code orthogonality (α) is either caused by time dispersion (as a result of multipath propagation), nonorthogonal code sets, or asynchronous signals arriving at the receiver [27], [28], as well as a combination of these effects. This directly impacts the level of multiple-access interference (MAI) in terms of self-interference. Here, $\alpha = 0$ represents complete code orthogonality and $\alpha = 1$ represents a complete loss of orthogonality.

Beam efficiency (ξ) accounts for power spilled into adjacent beams, which increases cochannel interference. This is caused by the magnitude of cusping loss between beams, side-lobe levels, and angular spread in the channel and takes a value of between 0 and 1, where 1 represents complete efficiency. The impact of each of the terms is described in Section III-A.

Pilot signal power is the proportion of power allocated to the pilot signal ($1 - \beta$, where β is power allocated to the users). The pilot signal is used to transmit the *broadcast control channel* (BCCH) and the *paging channel* (PCH) [26]. It is allocated a separate code and is common to all users and, thus, is transmitted on a fixed-coverage antenna within the entire cell or sector. The pilot channel signal orthogonality is, therefore, equivalent to that of an omnisector transmission.

Traffic-loading fraction (γ) represents the net downlink traffic load where $\gamma = 1$ is the fully loaded condition.

Intracell path loss $(\mathrm{Lp}_{\mathrm{Intra}})$ models the total path loss experienced by transmissions from the user's own base station as a function of distance. Intercell path loss $\mathrm{Lp}_{\mathrm{Inter}}$ is the sum of path losses from surrounding base stations to the user. Here, a cell radius of 1 km three-tier network with a single-cell reuse distance and uniform user distribution has been used in these investigations (i.e., 18 interfering base stations), together with a power law path-loss model employing a path loss exponent of $n = 4$, which is deemed to be appropriate with a base station height of 10 m and mobile height of 2 m. These parameters are in line with W-CDMA system appraisals reported in [27] and [28].

Shadowing (χ) is modeled as a log-normal random variable with variance σ_{SH} that models the shadowing experienced by the user [31], [32]. The shadowing model is described in Section IV-F.

III. Analysis

In this section, a closed-form expression is developed, which enables the performance of switched-beam antennas to be ascertained. The equation incorporates the terms defined in the previous section and the form of the equation considers the total transmit power from each base station and, since the signals pass through a common channel on the downlink, power control to each individual user can be considered as ideal in this analysis.

The downlink intercell interference received by a user in a network of J interfering base stations with omnisector directional antennas is given by (2). This assumes long-term temporal averaging of the received signal, since fast fading effects have been omitted. The impact of shadowing is considered in Sections IV-F and G.

$$I_{\mathrm{InterOM}} = \chi_{\mathrm{InterOM}} \sum_{j=1}^{J} Lp_{\mathrm{Interj}} \cdot (\beta_j \cdot \gamma_j \cdot \alpha_{\mathrm{InterOMj}} + (1 - \beta_j) \cdot \alpha_{\mathrm{InterOMj}}) \quad (2)$$

where $\alpha_{\mathrm{InterOMj}}$ represents the intercell orthogonality factor with omnisector antennas at the jth interfering base station and χ_{InterOM} represents the instantaneous shadowing coefficient resulting from the J interfering base stations when operating with omnisector antennas.

Similarly, intracell interference can be computed with omnisector antennas by (3). Also, the inter- and intracell interference for cells using switched-beam antennas are computed from (4) and (5), respectively. Note that the $(1 - \beta)$ term in the equations represents the pilot power fraction that does not reduce as a function of beamwidth, since it is required to be transmitted simultaneously across the entire coverage area.

$$I_{\mathrm{IntraOM}} = \chi_{\mathrm{IntraOM}} \mathrm{Lp}_{\mathrm{Intra}} \cdot (\beta \cdot \gamma \cdot \alpha_{\mathrm{IntraOM}} + (1 - \beta) \cdot \alpha_{\mathrm{IntraOM}}) \quad (3)$$

$$I_{\mathrm{InterSB}} = \chi_{\mathrm{InterSB}} \sum_{j=1}^{J} \mathrm{Lp}_{\mathrm{Interj}} \cdot \left[\left(\frac{\beta_j \cdot \gamma_j \cdot \alpha_{\mathrm{InterSBj}}}{N_j \cdot \xi_j} \right) + (1 - \beta_j) \cdot \alpha_{\mathrm{InterPilotj}} \right] \quad (4)$$

$$I_{\mathrm{IntraSB}} = \chi_{\mathrm{IntraSB}} \mathrm{Lp}_{\mathrm{Intra}} \cdot \left[\left(\frac{\beta \cdot \gamma \cdot \alpha_{\mathrm{IntraSB}}}{N \cdot \xi} \right) + (1 - \beta) \cdot \alpha_{\mathrm{IntraPilot}} \right] \quad (5)$$

where

- $\alpha_{\mathrm{IntraSB}}$ intracell orthogonality factor with switched-beam antennas;
- $\alpha_{\mathrm{IntraOM}}$ intracell orthogonality factor with omnisector antennas;
- $\alpha_{\mathrm{InterSB}}$ intercell orthogonality factor with switched-beam antennas;
- $\alpha_{\mathrm{IntraPilot}}$ intracell orthogonality factor of the omnisector pilot channel;
- $\alpha_{\mathrm{InterPilot}}$ intercell orthogonality factor of the omnisector pilot channel;
- χ_{IntraSB} shadowing coefficient from the user's base station operating with a switched-beam antenna;
- χ_{IntraOM} shadowing coefficient from the user's base station operating with an omnisector antenna;
- χ_{InterSB} shadowing coefficient from the interfering base stations operating with switched-beam antennas;
- χ_{InterOM} shadowing coefficient from the interfering base stations operating with omnisector antennas;
- N number of equal beamwidth beams.

Thus, the *interference reduction ratio* (IRR) obtained by employing a switch-beam antenna compared to the single omnisector case is given by (6). In interference-limited networks, a

TABLE I
W-CDMA SWITCHED-BEAM TEST PARAMETERS

Parameter	Value
Number of Beams (N)	1-32
Traffic Loading Factor (γ)	100%
Pilot Signal Power Fraction (1-β)	20%
α_{InterOM}	1
α_{InterSB}	1
α_{IntraOM}	0.4
α_{IntraSB}	See table 2
Beam Efficiency (ξ)	See table 2
Total Inter-cell Path Loss$^{\lceil 1}$(Lp_{Inter})	90dB
Intra-cell Path Loss (Lp_{Intra})	80dB
χ_{InterSB}, χ_{IntraOM}, χ_{IntraSB}, χ_{InterOM}	0dB

TABLE II
W-CDMA SWITCHED BEAM TEST PARAMETERS

N	Ideal Azimuth	α_{IntraSB}	Beam Efficiency ξ
Omni-sector	120°	0.4	90%
4	30°	0.2	90%
8	15°	0.1	90%
16	7.5°	0.05	65%
24	5°	0.025	40%
32	3.75°	0.012	27.5%

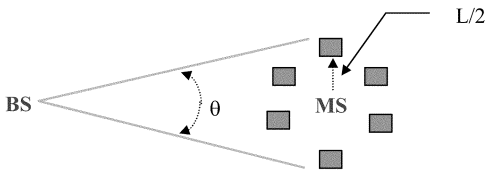

Fig. 2. Ring of scatterers.

reduction in interference can be translated into a capacity gain. Hence, (6) also gives an indication of the capacity gain that is obtainable from switched-beam antennas. This equation compares the total interference power received by the user in a network employing omnisector antennas with that of a network employing switched-beam antenna systems in each sector and assumes the received powers combine linearly.

$$\text{IRR} = \frac{I_{\text{InterOM}} + I_{\text{IntraOM}}}{I_{\text{InterSB}} + I_{\text{IntraSB}}}. \tag{6}$$

IV. PERFORMANCE OF SWITCHED-BEAM ANTENNAS IN W-CDMA

In this section, numerical results are obtained for the expression developed above. The downlink IRR observed by employing a switched-beam antenna in the central cell compared to a 120° fixed coverage omnisector case. The expression is evaluated as a function of the following system parameters and are presented in the forthcoming sections:

- number of beams;
- beam efficiency;
- traffic loading;
- pilot power fraction;
- path loss;
- code orthogonality;
- shadowing variance;
- shadowing correlation.

A. IRR Versus Number of Beams and Beam Efficiency

This evaluation is initially carried out using the system parameters given in Table I, where the number of beams is incremented from 1 (omnisector) to the extreme case of $N = 32$. The path-loss values have been chosen to represent a user located midway between the base station and cell boundary using the path-loss model stated in Section II. The shadowing coefficients χ are set to 0 dB for this investigation. The impact of shadowing is studied in Sections IV-F and G. A representative value of pilot power fraction is specified in [26]; however, actual values are currently unavailable in the literature. For this investigation, the network is assumed to be fully loaded ($\gamma = 1$). $\alpha_{\text{InterOM}} = 1$ is assumed since W-CDMA utilizes an asynchronous air interface; hence, intercell codes will not be synchronized, rendering the possibility of worst-case cross-correlation properties between them. Since this value is due to asynchronous codes and not time dispersion, employing a narrower beam will not reduce α_{InterSB}. The value of α_{IntraOM} for an omnisector antenna in Table I has been computed in [26] and is representative of a macrocell with a 120° antenna. The derivation of the remaining values is now described.

The primary mechanism for orthogonality loss is, in this case, time dispersion [27]. By reducing the beamwidth, an improvement in orthogonality may be expected and is estimated in Table II for various beamwidths (Bw) assuming a chipping rate of 3.84 Mc/s, base station antenna mounted above rooftop height, and the scatterers modeled as a ring of radius $L/2$ around the user (where L is the system's range resolution given by $L = c \cdot T_c$ and the speed of light $c = 3 \times 10^8$ m/s) shown in Fig. 2. The resulting value is estimated by

$$\alpha_{\text{IntraSB}} = \frac{\alpha_{\text{IntraOM}} \cdot Bw}{120°}. \tag{7}$$

The loss of orthogonality is manifested when the propagation delay between two impulses arriving at the receiver is less than the chip period, T_c. Consequently, the RAKE receiver cannot resolve the paths and the fading that results, which causes interference at the detector output. The delay corresponds to a path length difference of $\Delta d \leq L$. In the case of W-CDMA, $T_c = 260.4$ ns and, therefore, $L = 78$ m. Scatterers within the area defined by d, d_1, and d_2 in Fig. 3, cause these path-length differences and scatterers outside the area will cause path-length differences of $\Delta d > L$, which are resolvable by the RAKE receiver.

For a mobile station located at $d = 500$ m from the base station, the model in Fig. 3 yields $d_1 = 145$ m and $d_2 = 39$ m. By reducing the antenna beamwidth, the number of scatterers

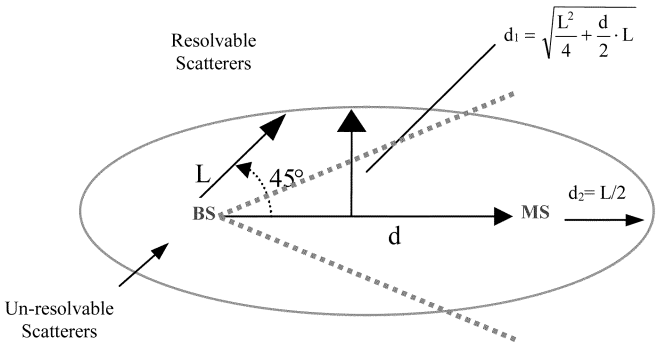

Fig. 3. Locus of scatterers causing othogonality loss (. . . . . 30° beamwidth).

illuminated inside the locus will reduce, but this can only occur when the beamwidth significantly reduces coverage within the locus. Assuming uniformly distributed scatterers throughout the coverage area, the required beamwidth (θ) to reduce the number of scatterers by 50% is given by (8) and yields $\theta = 30^\circ$ for the above example. As a consequence of reducing the scattering within the locus, the number of unresolvable multipaths is reduced, thus helping to preserve orthogonality. Note, however, that by employing narrow-beamwidth antennas, the resolvable multipaths present at the RAKE receiver are also reduced, which will cause the achievable path diversity gain to diminish. A beamwidth of $\theta = 30^\circ$ is achievable with a uniformly weighted four-element linear array.

$$\theta = 2 \cdot \tan^{-1}\left[\frac{2 \cdot \sqrt{\frac{L^2}{4} + \frac{d_1}{2} \cdot L}}{d_1}\right]. \tag{8}$$

Using the above analysis, the orthogonality factors are given in Table II for a number of beamwidths. This table also shows the beam efficiencies that have been used in this investigation. Three parameters contribute to beam efficiency: radiation pattern loss (L_{Rad}), beam cusp loss (L_{Cusp}), and angular spread loss (L_{AS}). The cumulative effect is given by

$$\xi = (1 - L_{\mathrm{Rad}}) + (1 - L_{\mathrm{Cusp}}) + (1 - L_{\mathrm{AS}}). \tag{9}$$

Radiation pattern loss (L_{Rad}) is defined by (10) [33] and describes the power radiated through the main beam compared to the total radiated power. The theoretical "top hat" antenna pattern that does not possess sidelobes would, therefore, yield $L_{\mathrm{Rad}} = 1$.

$$L_{\mathrm{Rad}} = 1 - \frac{P_{\mathrm{Main}}}{P_{\mathrm{Total}}}. \tag{10}$$

$\mathrm{P}_{\mathrm{Main}}$ is the power transmitted in the main beam (defined as the area between the first two nulls) and P_{Total} is the total transmitted power. The above definition considers a three-dimensional (3-D) radiation pattern but is equally valid for the azimuth pattern assuming a uniform radiation pattern in elevation. The azimuth radiation pattern for an eight-element uniform linear array (ULA) with $\lambda/2$ element spacing, shown in Fig. 4, yields L_{Rad} to be 90%, which has been used throughout this analysis.

The presence of adjacent beams overlapping with the wanted main beam will further degrade the beam efficiency (L_{Cusp}). A

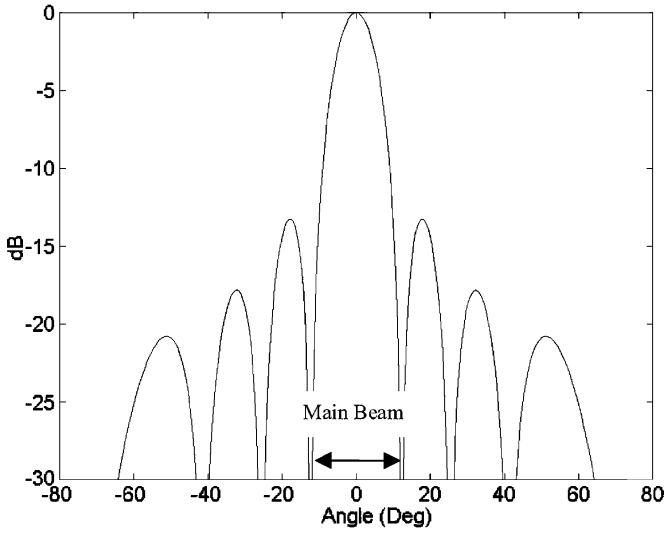

Fig. 4. Beam efficiency (eight-element ULA).

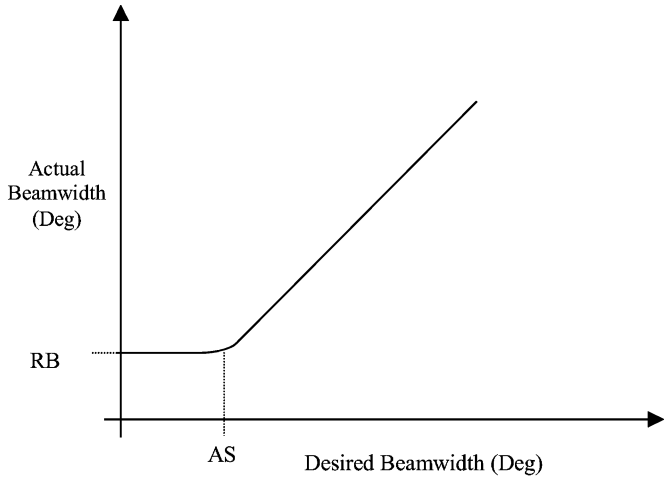

Fig. 5. Beamwidth limitation due to residue angular spread.

cusping loss of 4 dB is a typical figure (although it can be reduced as reported in [19]). The impact of cusping loss on system performance depends upon the angular position of the mobile station. In order to optimize beam efficiency, it is desirable to minimize L_{Cusp}. This would, however, compromise quality of service to users located in the cusp region and, therefore, highlights a design tradeoff. For simplicity, cusping loss is assumed to be ideal $(L_{\mathrm{Cusp}} = 0)$ in this analysis; thus, further analysis is required to fully model the impact of cusping loss.

Once the beamwidth becomes smaller than the largest angular spread, this later effect dominates, causing energy to spread out of the main beam with the possibility of increasing interference levels to cochannel users. This residue beamwidth (RB) is illustrated in Fig. 5 and can be defined as the angular spread (AS) observed when an infinitely narrow beam excites the channel. Fig. 5 shows that the beamwidth is limited by the angular spread. This is reflected in Table II, where beam efficiency rapidly reduces for beamwidths of less than the angular spread. Throughout this investigation, an angular spread of 10° is considered to be representative of an urban environment and falls within the range reported in [34]. L_{AS}

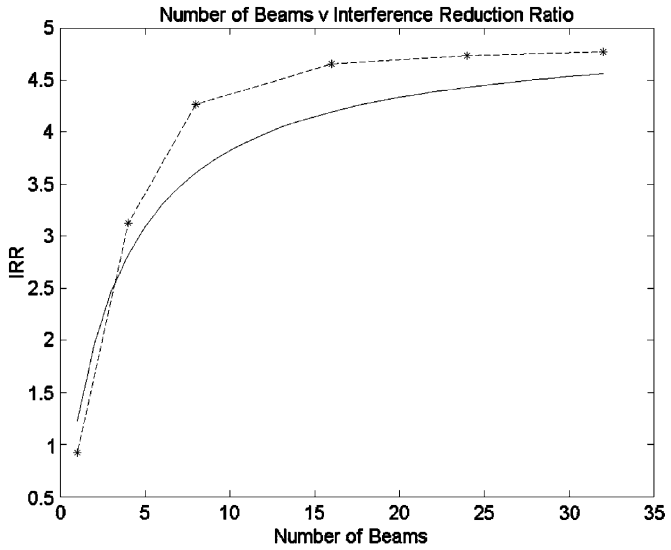

Fig. 6. IRR versus the number of beams (user located midway between BS and cell boundary). See Tables I and II for system parameters. ___ = ideal and − − ∗ − − − − = realistic .

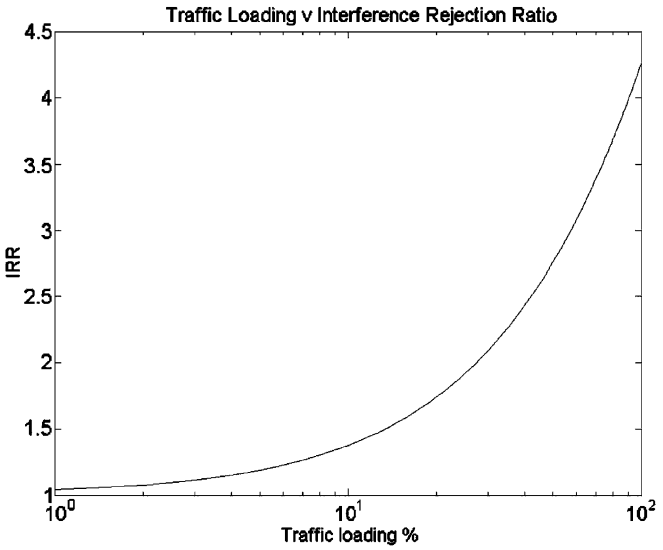

Fig. 7. IRR versus traffic loading (an eight-beam antenna system is employed with the user located midway between the BS and cell boundary). System parameters are given in Tables I and II.

is computed by (11), where Bw is the azimuth beamwidth and AS the angular spread.

$$L_{\mathrm{AS}} = 1 - \frac{Bw}{\mathrm{AS}}. \tag{11}$$

Fig. 6 illustrates the achievable IRR computed using the above analysis as the number of equally spaced beams within the sector is increased. Initially, it is assumed that beam efficiency and $\alpha_{\mathrm{IntraSB}}$ stay constant (at levels of 90% and 0.4, respectively) as the number of beams increases and yields the idealistic curve shown. In a practical system, the beamwidth efficiency and $\alpha_{\mathrm{IntraSB}}$ will vary with beamwidth, as shown in Table II. The realistic curve shown in this figure reflects a practical system performance and shows that an optimum IRR is achieved when 16 beams are used, each having a 3-dB beamwidth of 7.5°. This is realized with a 16–element ULA. The figure also shows that a similar performance is attainable with eight beams of 15°. This is a more practical solution as an eight-element ULA is required, therefore reducing the system cost, complexity, wind-loading, and cabling associated with a larger array. Note that this figure shows that little performance gain is achieved by increasing the number of beams above 16. Performance with relatively small beamwidths is highly dependent upon the level of angular spread. Here it has been stated that 10° of angular spread is assumed. Environments exhibiting higher values of angular spread will exhibit a reduction in IRR since L_{AS} will be increased. In severe cases, performance gain may be negligible.

B. Traffic Loading

In this section, the impact of traffic loading on the downlink IRR is investigated. The optimum number of beams for a practical system ($N = 8$) is used from the previous section with the associated system parameters in Tables I and II and the traffic loading factor γ is incremented from 1% to 100%. During normal operation, the system will be close to fully loaded and, assuming uniformly distributed users throughout the sector, all N beams are active. This was the system stated in the previous section. However, during quiet times, the system is fractionally loaded ($\gamma < 100\%$) and, consequently, only a few beams are active. In this case, the downlink IRR will be less since fewer users are present. The resulting curve of IRR is shown in Fig. 7 as a function of traffic loading. The increased effectiveness of switched-beam antennas as the load is increased is illustrated and yields an IRR of 4.25 (6.3 dB) in the fully loaded case, which corresponds to the optimum condition in Fig. 6. Galvan-Tejada and Gardiner also report a similar result in [35], where it is concluded that space-division multiple access is not efficient for low traffic loads, but is highly efficient for high-traffic scenarios.

C. Pilot Power Fraction

Fig. 8 presents the achievable IRR as a function of pilot power fraction when incremented from 0% (no pilot) to the impractical case of 100%, where only a pilot signal is transmitted (which precludes any user transmissions). The system parameters detailed in Tables I and II have been used in conjunction with an eight-beam system. For very low pilot powers ($< 20\%$), an IRR in excess of four is obtained. It is, therefore, desirable to minimize the pilot power fraction so that an optimum capacity gain is achieved (which is also desirable for optimal performance of networks that do not employ smart antennas systems).

D. Path Loss

Here, the impact of inter- and intracell path loss on IRR is investigated using the system parameters detailed in Tables I and II in conjunction with an eight-beam system. The inter- and intrapath losses are incremented in turn, from 70 dB through to 145 dB, therefore covering the following scenarios:

1) Mobiles close to the home base station with a large path loss from surrounding base stations;

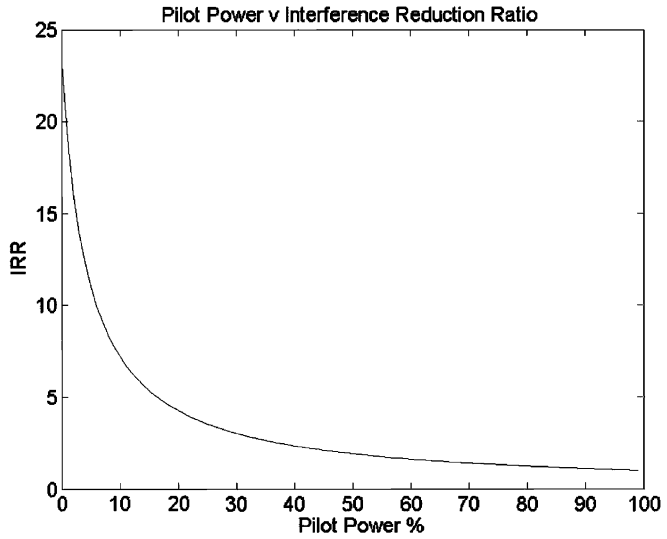

Fig. 8. IRR versus pilot power fraction (an eight-beam antenna system is employed with the user located midway between the BS and cell boundary). System parameters are given in Tables I and II.

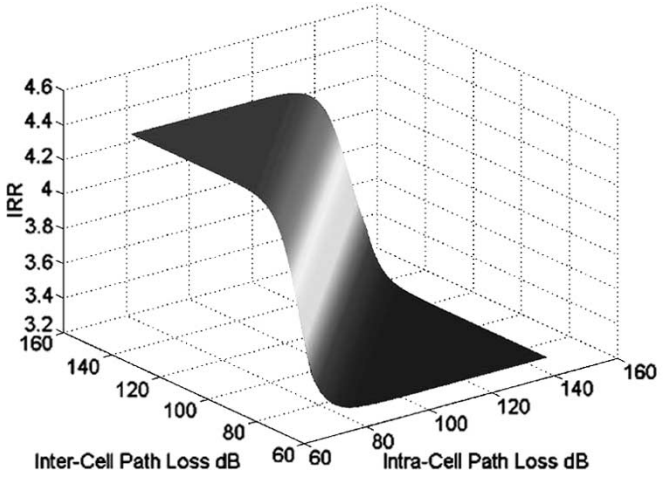

Fig. 9. IRR versus path loss (an eight-beam antenna system is employed). System parameters are given in Tables I and II.

2) Mobiles on the cell boundary with a comparable path loss to their own and surrounding base stations (handover region);
3) Mobiles that have a larger path loss to their own base station than neighboring base stations and should, therefore, hand over to the new cell.

Fig. 9 shows the optimum IRR is achieved when the intracell pathloss is small compared to intercell pathloss (scenario 1). As the user moves away, intercell path loss will decrease and intracell path loss will increase. Now, the nonorthogonal interference will dominate and IRR is reduced. For this region, the user is considered to be in a handover region (scenario 2). If soft handover is employed, strong intercell signals could be exploited to improve diversity gain and will not appear as capacity-limiting interference. In a softer handover scenario, diversity is more difficult to exploit since the two signals will have a higher correlation (although this does depend on the antenna topology and angular spread of the channel). In this case, three options exist.

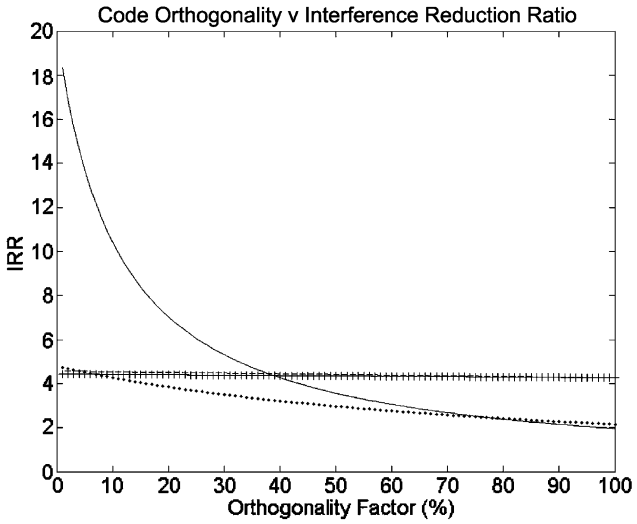

Fig. 10. IRR versus code orthogonality for a user located midway between the BS and cell boundary (an eight-beam antenna system is employed). System parameters are given in Tables I and II. $-\ .\ -\ .\ -$ is intracell user signal orthogonality, $+\ +\ +\ +$ is intercell user signal orthogonality, $\_$ is intracell pilot signal orthogonality, and . . . . . is intercell pilot-signal orthogonality.

- Adjacent asynchronous sectors employing a different scrambling code will be seen as interference.
- Adjacent sectors employing different scrambling codes will be detected as in soft handover, therefore giving some diversity gain.
- Adjacent synchronous sectors will have little impact on system performance since code orthogonality will be preserved.

Consequently, Fig. 9 shows that optimum performance is obtained for users with high received signal strengths, which will be those users within the cell boundary.

E. Code Orthogonality

The two scenarios presented here illustrate the impact of code orthogonality on IRR. The first considers the user located approximately midway between the base station and cell boundary, as in the previous sections, and the second considers the user close to the cell boundary ($\mathrm{Lp}_{\mathrm{Inter}} = 90$ dB and $\mathrm{Lp}_{\mathrm{Intra}} = 87$ dB). In both cases, an eight-beam system is utilized in conjunction with the parameters in Tables I and II. For each of the scenarios, four curves are generated by fixing the orthogonality factors at the values given in the table and incrementing the parameter in question from 0 to 1. Note that the orthogonality factors relating to the omnisector case are constant, as this forms the reference case for comparison.

The impact of user and pilot signal orthogonality on IRR is shown in Fig. 10 for a user located midway between the base station and cell boundary. Similarly, this is shown in Fig. 10 for a user located at the cell boundary. Fig. 10 shows IRR to have a high dependence on the home–cell pilot signal orthogonality factor $(\alpha_{\mathrm{IntraPilot}})$. It is, therefore, highly desirable to attempt to preserve the orthogonality of pilot signal transmissions. This figure also shows much less dependency on intercell transmissions, since the home base station path loss is lower than that of neighboring base stations, making the intercell signal parameters dominant.

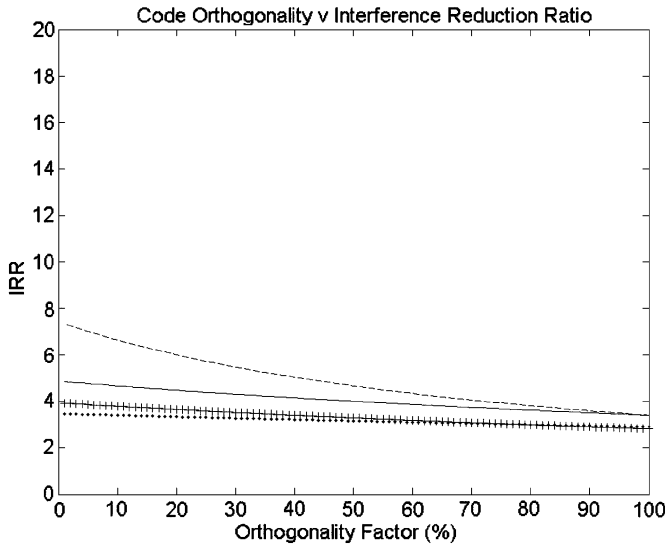

Fig. 11. IRR versus code orthogonality for a user located close to BS and cell boundary (an eight-beam antenna system is employed). System parameters are given in Tables I and II. $-\,.\,-\,.\,-$ is intracell user signal orthogonality, $+\,+\,+\,+$ is ntercell user signal orthogonality, $\_\_$ is intracell pilot signal orthogonality, and . . . . . is intercell pilot-signal orthogonality.

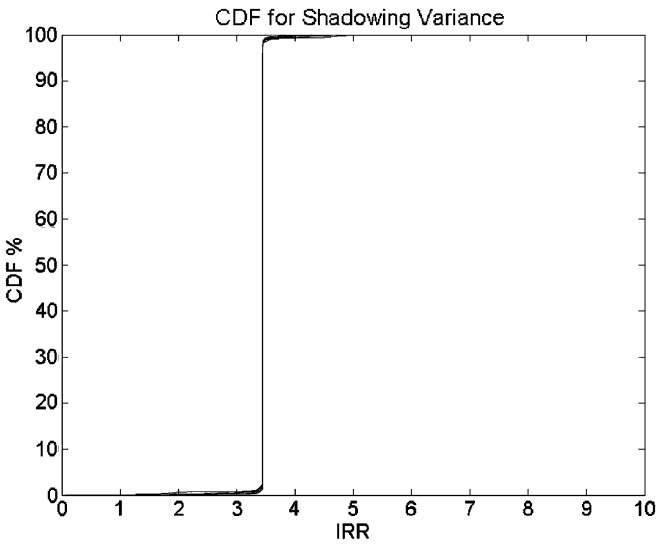

Fig. 12. Cumulative distribution function (cdf) of IRR for $\sigma_{\mathrm{SH}} = 6 - 12$ dB. (See Tables I and II for system parameters.)

Fig. 11 shows an increased dependence on the intercell transmissions due to the user being located at the cell boundary. This is also reflected in the results of Section IV-D, where a reduction in IRR is observed for users located around the cell border.

F. Shadowing Variance

This section evaluates the impact of shadowing variance on IRR. Shadowing is incorporated into the computation of instantaneous IRR by modeling shadowing coefficients χ_{InterOM}, χ_{IntraOM}, χ_{InterSB}, and χ_{IntraSB} as log-normal random variables [29], which are parameters in (2)–(5). Since there are J interfering base stations (where $J = 18$ here), χ_{InterOM} and χ_{InterSB} are the sum of J log-normal random variables. The sum of log-normal random samples is approximately a log-normal probability density function (pdf), assuming all J pdfs are identical [29]. This is a reasonable assumption if a homogeneous propagation environment is assumed. A further simplification is possible by assuming that the difference in shadowing variance is negligible when changing from an omni to directional antenna is negligible. This is considered reasonable since shadowing is caused by clutter surrounding the mobile; thus, as long as the antenna beamwidth is larger than the angular spread of the channel, the shadowing characteristics will be independent of the base station antenna. This investigation employs an eight-element ULA, which has a beamwidth that is larger than the angular spread, as shown in Section IV-A and [34].

Thus, treating χ_{InterOM}, χ_{IntraOM}, χ_{InterSB}, and χ_{IntraSB} as independent log-normal random variables with variance $6\,\mathrm{dB} \leq \sigma_{\mathrm{SH}} \leq 12$ dB and computing the average IRR over 100 000 trials for each value of σ_{SH} for a system using an eight-element ULA and the parameters given in Tables I and II and Fig. 12 is obtained. The figure shows the cdf for each value of σ_{SH}. It is evident from the figure that little variation exists over the range of σ_{SH} considered.

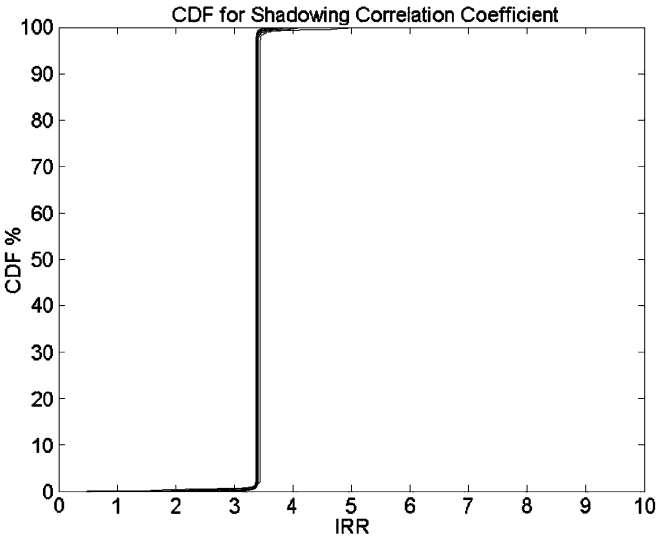

Fig. 13. The cdf of IRR for $\rho_{\mathrm{SH}} = 0 - 1$. (See Tables I and II for system parameters.)

G. Shadowing Correlation

The investigation into shadowing has so far assumed uncorrelated shadowing coefficients; however, in practice, a degree of correlation ρ_{SH} exists between each shadowing component where $\rho_{\mathrm{SH}} \geq 0.35$ [30]. The study is now extended to incorporate ρ_{SH} as follows. It is assumed here that the correlation coefficient ρ_{SH} is the same between all $J+1$ transmissions that contribute to the shadowing components. Thus, the $\{J+1 \times J+1\}$ correlation matrix $\mathbf{R_{SH}}$, which describes the correlation between all $J+1$ shadowing components, is given by

$$\mathbf{R_{SH}} = \begin{bmatrix} 1 & \rho_{\mathrm{SH}} & \cdots & \rho_{\mathrm{SH}} \\ \rho_{\mathrm{SH}} & \ddots & \ddots & \vdots \\ \vdots & \ddots & \ddots & \rho_{\mathrm{SH}} \\ \rho_{\mathrm{SH}} & \cdots & \rho_{\mathrm{SH}} & 1 \end{bmatrix}. \tag{12}$$

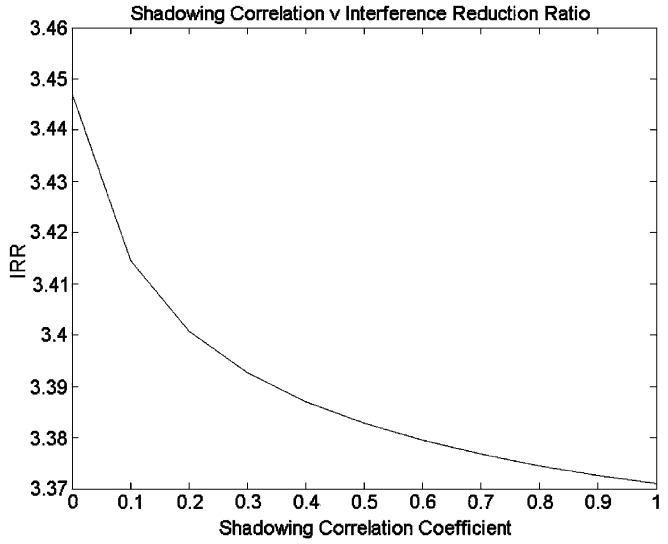

Fig. 14. IRR versus ρ_{SH}. (See Tables I and II for system parameters.)

The $J+1$ vector of correlated shadowing components χ_C is obtained by multiplying the $J+1$ vector of independent shadowing components χ by $\sqrt{\mathbf{R_{SH}}}$, as given by

$$\chi_{\mathrm{C}} = \sqrt{\mathbf{R_{SH}}}\chi. \tag{13}$$

The correlated shadowing coefficients are then used in the computation in the same way as in Section IV-F. By repeating the calculation 100 000 times for $0 \leq \rho_{\mathrm{SH}} \leq 1$ and plotting the cdf in Fig. 13 is obtained. This figure shows a negligible variation of IRR over the range of ρ_{SH}. Fig. 14 is obtained by taking the mean value of IRR obtained over the range of ρ_{SH}. This shows IRR to reduce by 2.6% as ρ_{SH} is increased.

V. Conclusion

A closed-form expression for evaluating the downlink interference reduction in W-CDMA networks employing switched-beam antennas has been introduced. Uniquely, the expression incorporates a number of parameters enabling a realistic level of multiple access interference to be computed and features specific to W-CDMA to be assessed.

The expression has been evaluated in terms of the number of beams employed in a theoretical and ideal system along with the impact of beam efficiency, traffic loading, pilot-power fraction, path loss, code orthogonality, and shadowing. The results show that an eight-beam system can reduce downlink interference by a factor of 6 dB compared to a central cell employing a 120° omnisector antenna. Furthermore, it is shown that IRR diminishes once the beamwidth is smaller than the angular spread of the channel. The results also show that the IRR is maximized for a fully loaded network. The amount of interference experienced by a user during fractionally loaded periods is relatively small, making the impact of employing a switched-beam antenna system much less. The analysis also shows the impact of pilot-power fraction to be a limiting factor in the attainable IRR. This highlights the need for close control of the pilot signal power since large improvements in IRR can be obtained, particularly when the pilot power fraction is less than 30%. The investigation into the impact of path loss has considered three scenarios.

- Adjacent asynchronous sectors employing a different scrambling code will be seen as interference.
- Adjacent sectors employing different scrambling codes will be detected as in soft handover, therefore giving some diversity gain.
- Adjacent synchronous sectors will have little impact on system performance since code orthogonality will be preserved.

The results show that a mobile will experience the optimum IRR when path loss to the home base station is smaller than to neighboring base stations (scenario 1). Users in the handover region (scenario 2) may exploit soft handover in order to improve performance. Code orthononality has also been considered in this analysis, where it is shown that IRR is particularly sensitive to pilot signal orthogonality. This highlights the importance of preserving pilot-signal orthogonality as well as minimizing the pilot power fraction in order to attain optimum performance. Finally, shadowing has been investigated in terms of variance and correlation. These investigations have shown that shadowing variance has a negligible impact on IRR and that, as the correlation between shadowing component is increased, IRR decreases by 2.6%.

Using the above results, the following recommendations can be made with regard to the deployment of switched-beam antenna systems on the downlink of W-CDMA systems.

- From the system and network parameters used in the analysis, an eight-beam system offers optimum performance (see Fig. 6).
- It is highly desirable to control the pilot–power fraction and to attempt to preserve pilot signal code orthogonality as the performance shows particularly sensitivity to these parameters. Consequently, systems should be deployed with regulated pilot transmission powers and optimized coverage to reduce radiation into adjacent cells.

Acknowledgment

The authors would like to thank M. Hunukumbure for his analysis of code orthogonality and E. Bonek and A. Nix for their useful comments on the work presented here.

References

[1] S. C. Swales, M. A. Beach, D. Edwards, and J. P. McGeehan, "The performance enhancement of multi-beam adaptive base station antennas for cellular land mobile radio systems," *IEEE Trans. Veh. Technol.*, vol. 39, pp. 56–67, Feb. 1990.

[2] G. Tsoulos, "Smart antennas for mobile communication systems: Benefits and challenges," *Electron. Commun. J.*, vol. 11, no. 2, pp. 84–94, 1999.

[3] G. Tsoulos, G. Athanasiadou, and R. Piechocki, "Low-complexity smart antenna methods for third-generation W-CDMA systems," *IEEE Trans. Veh. Technol.*, vol. 49, pp. 2382–2396, Nov. 2000.

[4] T. Matsumoto, S. Nishioka, and D. Hodder, "Beam-selection performance analysis of a switched multibeam antenna system in mobile communications environment," *IEEE Trans. Veh. Technol.*, vol. 46, pp. 10–20, Feb. 1997.

[5] A. Paulraj and C. Papadias, "Space–time processing for wireless communications," *IEEE Signal Processing Mag.*, vol. 14, pp. 49–83, Nov. 1997.

[6] *Proc. Second Workshop Smart Antennas in Wireless Mobile Communications*, July 20–21, 1995.

[7] H. Noualc, "Switched beam adaptive antenna demonstrator for UMTS data rates," in *Proc. Ninth Virginia Tech/MPRG Symp. Wireless Personal Commun.*, June 2–4, 1999, pp. 85–93.
[8] Y. Li, M. Feuerstein, and D. Residink, "Performance evaluation of a cellular base station multi-beam antenna," *IEEE Trans. Veh. Technol.*, vol. 46, pp. 1–9, Feb. 1997.
[9] T. MacNamara, "Simplified design procedures for butler matrices incorporating 90 degree hybrids," *Inst. Elect. Eng. Proc.*, pt. H, vol. 134, no. 1, pp. 50–54, 1987.
[10] R. C. Hansen, *Microwave Scanning Arrays*. New York: Academic, 1966, vol. 3, pp. 258–263.
[11] J. Tui, *Digital Microwave Receivers, Theory and Concepts*. Norwood, MA: Artech House, 1989, pp. 250–253.
[12] D. Archer, "Lens-fed multiple beam arrays," *Microwave J.*, pp. 171–195, 1984.
[13] M. Beach, C. Simmonds, P. Howard, and P. Darwood, "European smart antenna test bed—Field trials results," *IEICE Trans. Commun.*, vol. E84-B, no. 9, pp. 2348–2356, 2001.
[14] Y. Guo, S. Vadgama, and Y. Tanaka, "Advanced base station technologies for UTRAN," *Electron. Commun. Eng. J.*, vol. 12, no. 3, pp. 123–132, 2000.
[15] M. Skolnik, *Introduction to Radar Systems*, 2nd ed. New York: McGraw-Hill, 1980, p. 284.
[16] P. Mogensen, P. Zetterberg, H. Dam, P. Espensen, and F. Fredriksen, "Algorithms and Antenna Array Recommendations," TSUNAMI II Tech. Rep. AC020/AUC/A1.2/DR/P/005/b1, 1997.
[17] T. Moorti and A. Paulraj, "Performance of switched beam systems in cellular base stations," in *Proc. IEEE ASILOMAR 29*, 1995, pp. 388–392.
[18] T. Bachelier, J. Santé, and G. Cegetel, "Influence of mobility on capacity of DCS network using switched-beam antenna," in *Intelligent Antenna Technology for Mobile Communications Symposium*. Surrey, U.K.: Univ. of Surrey Press, 1997.
[19] C. Ward, D. Adams, F. Wilson, and A. Bush, "The live-air trial of a multi-beam cellular base station antenna system," in *Proc. Inst. Elect. Eng. Nat. Conf. Antennas and Propagation*, 1999, pp. 169–172.
[20] M. Ho, G. Stüber, and M. Austin, "Performance of switch beam smart antennas for cellular radio systems," *IEEE Trans. Veh. Technol.*, vol. 47, pp. 10–19, Feb. 1998.
[21] M. Beach, B. Allen, and P. Karlsson, "Spatial decorrelation of frequency division duplex links," *Electron. Lett.*, vol. 36, no. 22, pp. 1884–1885, 2000.
[22] M. Beach, B. Allen, and P. Karlsson, "Spatial channel characterization for smart antenna solutions in FDD wireless networks," *IEEE Trans. Antennas Propagat.*, vol. 52, pp. 252–262, Jan. 2004.
[23] E. Tirrola and J. Ylitalo, "Performance evaluation of fixed-beam beamforming in WCDMA downlink," in *Proc. IEEE VTC'00*, Tokyo, Japan, 2000.
[24] T. Mootri, R. Stützle, and A. Paulraj, "Performance of a fixed-beam system in the IS-95 CDMA forward link," *Eur. Trans. Telecommun.*, vol. 9, no. 4, pp. 361–370, 1998.
[25] B. Allen, M. Beach, and P. Karlsson, "Analysis of smart antenna outage in UTRA FDD networks," *Electron. Lett.*, vol. 38, no. 1, pp. 2–3, 2002.
[26] T. Ojanperä and R. Prasad, *Wideband CDMA for Third Generation Mobile Communications*. Norwood, MA: Artech House, 1998, pp. 226–229.
[27] F. Adachi, "Effects of orthogonal spreading and rake combining on DS-CDMA forward link in mobile radio," *IEICE Trans. Commun.*, vol. E80-B, no. 11, pp. 1703–1712, 1997.
[28] M. Hunukumbure, M. A. Beach, and B. H. Allen, "On the down-link orthogonality factor in UTRA FDD systems," *Electron. Lett.*, vol. 38, no. 4, pp. 196–197, 2002.
[29] P. Stevens, "Operator design and planning issues for UMTS networks," in *Proc. UMTS—The R&D Challenges Col.*, 1998.
[30] S. Dehghan, D. Lister, R. Owen, and P. Jones, "W-CDMA capacity and planning," *Electron. Commun. E. J.*, vol. 12, no. 3, pp. 101–118.
[31] J. Cavers, *Mobile Channel Characteristics*. Norwell, MA: Kluwer, 2000, pp. 15–22.
[32] S. Saunders, *Antennas and Propagation for Wireless Communication Systems*. New York: Wiley, 1999, p. 172.
[33] C. Balanis, *Antenna Theory, Analysis and Design*. New York: Wiley, 1982, p. 46.
[34] B. Allen, J. Webber, P. Karlsson, and M. Beach, "UMTS spatio-temporal propagation trial results," in *Proc. Inst. Elect. Eng. Int. Conf. Antennas and Propagation*, Apr. 17–20, 2001.
[35] G. Galvan-Tejada and J. Gardiner, "Theoretical model to determine the blocking probability for SDMA systems," *IEEE Trans. Veh. Technol.*, vol. 50, pp. 1279–1288, Sept. 2001.

Ben Allen (M'04) received the M.Sc. and Ph.D. degrees at the University of Bristol, Bristol, U.K., in 1997 and 2001, respectively.

He was with Nortel Networks, Paignton, Devon, U.K., working on their wireless local loop program and in 2001 he was with Tait Electronics, Christchurch, New Zealand, where he participated in the Australasian Space–Time Array Research collaboration. He now is a Lecturer with the Centre for Telecommunications Research, Kings College, London, U.K., where his research interests include space–time and multiple-input–multiple-output (MIMO) communications, smart-antenna technologies, and ultrawide-band (UWB) wireless systems. He has published numerous journal and conference papers in the above areas.

Dr. Allen is a Member of the Institution of Electrical Engineers (IEE).

Mark Beach (A'91) received the Ph.D. degree for research addressing the application of smart antennas to global positioning systems (GPS) from the University of Bristol, Bristol, U.K.

He joined the University of Bristol as a Member of Academic Staff in 1989, where he currently is Professor of Radio Systems Engineering. His research interest in smart-antenna techniques has continued with the application of dual array techniques (MIMO architectures) to high-performance wireless networks. Further, he has conducted novel research in the area of analog radio frequency (RF) technologies for software definable, or reconfigurable, radio, such as linearized mixers and tunable RF filters under E.U. projects such as TRUST and SCOUT.

Dr. Beach is an active Member of the Institution of Electrical Engineers Professional Network on Antennas and Propagation, as well as an Editor for the IEEE TRANSACTIONS ON WIRELESS COMMUNICATIONS.